DOI:
10.1021/acs.molpharmaceut.1c00680

Document Version
Peer reviewed version

Targeting the Amyloid with [^{18}F]AV-45 for Medullary Thyroid Carcinoma PET/CT Imaging: A Pilot Clinical Study

Chun Li[#], Pengxin Zhang[†], Ruirui Nie[#], Xiaoyan Gong[#], Jinghui Xie[#], Zilin Yu[*], Chengdong Wang[#], Hua Zhang, [#] Ran Yan[*], Zhi Lu[#]

[#]Department of Nuclear Medicine, First Affiliated Hospital of Dalian Medical University, People's Republic of China, 116021;

[†]Department of Pathology, First Affiliated Hospital of Dalian Medical University, People's Republic of China, 116021;

[*]King's College London, School of Biomedical Engineering and Imaging Sciences, St. Thomas' Hospital, SE1 7EH, London, United Kingdom.

Abstract

Medullary thyroid carcinoma (MTC) is a malignant neuroendocrine tumor with high recurrent rate. Amyloid plaques formed from the misfolding of calcitonin is the key characteristics of MTC. Herein, we conducted a first in human pilot clinical study by applying the β-amyloid specific radiotracer, [^{18}F]AV-45 to the PET/CT imaging of MTC. The presence of amyloid plaques in the tumor tissue sections from five MTC patients were confirmed by both H&E and Congo Red staining. [^{18}F]AV-45 selectively accumulated in the amyloid plaques in the continued tumor tissue sections with similar distribution pattern to the H&E and Congo Red staining. In addition, the [^{18}F]AV-45 uptake can be largely blocked by its non-radioactive reference compound. The [^{18}F]AV-45 accumulation in the thyroids, neck lymph nodes, and muscle in healthy human subjects is close to background indicated by PET/CT imaging. In the comparison PET/CT imaging study of a recurrent MTC patient, [^{18}F]FDG showed elevated uptake by multiple neck lymph nodes. In contrast, only one of these neck lymph nodes had increased [^{18}F]AV-45 uptake. Post-operative histopathological analysis confirmed the [^{18}F]AV-45 PET positive lymph node as MTC with amyloid deposition. While, other [^{18}F]FDG positive lymph nodes were free from MTC and amyloid plaques. Thus, [^{18}F]AV-45 showed the promise for the clinical PET/CT imaging of MTC.

Key words: Medullary thyroid carcinoma, [^{18}F]AV-45, amyloid, PET/CT

Introduction

Medullary thyroid carcinoma (MTC) is a type of malignant neuroendocrine tumor derived from parafollicular C cells in the thyroid gland.[1] Although it only accounts for around 1~2% of thyroid cancers, MTC causes 13.4% of all thyroid-related deaths.[2] Nearly 50% of MTC patients develop recurrent lesions and the prognosis is closely related to MTC development stage.[3] AJCC stage I, II, III MTC patients have

10-year survival rates of 100%, 93%, and 71%, respectively but drastically decreased to 21% in AJCC stage IV MTC patients. Therefore, early diagnosis is vital for the survival of MTC patients.[3]

Currently, the invasive fine needle aspiration cytology (FNAC) is still the gold standard of MTC diagnosis with detection rate about 50%.[4] Conventional anatomic imaging techniques such as neck ultrasonography (US), contrast-enhanced (CT), and Magnetic resonance imaging (MRI) are used to detect MTC metastatic lesions.[5] However, it is challenging for these morphological imaging modalities to visualise lymph node lesions and small liver metastasis.[5] Several single-photon emission computed tomography (SPECT) tracers, such as [^{99m}Tc](V)-DMSA, [^{123}I]-MIBG, and [^{111}In]-pentetreotide have been attempted to image recurrent MTC but failed to provide sufficient sensitivity to localise the metastatic lesions.[6,7]

Positron emission tomography (PET) that measures cancer-associated biochemical variations is considered a superior functional imaging technique offering higher spatial resolution and better image quality of malignant lesions. Several MTC PET imaging comparison studies with [^{18}F]FDG, [^{18}F]FDOPA, and [^{68}Ga]-somatostatin conclude that [^{18}F]FDOPA measuring the increased activity of L-type amino acid transporter 1 has the best diagnostic performance among these three PET tracers.[8,9] [^{18}F]FDOPA has been recommended by the European Association of Nuclear Medicine (EANM) as first-line procedure for diagnosis of MTC with PET, if available.[10] However, the availability of [^{18}F]FDOPA is very limited to only a handful of PET centres worldwide due to its challenging radiosynthesis, prolonged preparation time, and low radiochemical yields.[11]

Amyloid deposition is associated with many pathologically unrelated human diseases such as Alzheimer, Parkinson, and Huntington diseases as well as MTC.[12,15] Although originated from the misfolding of different proteins, these unrelated amyloid plaques share similar β-sheet structure.[13,15] MTC contains amyloid deposition formed from misfolded calcitonins which are rich in β-sheet structure.[15] Thus, we hypothesis that PET tracer such as [^{18}F]AV-45 (florbetapir)[14] for imaging amyloid burden in Alzheimer diseases can be applied to MTC diagnosis. In this first in human clinical study, we report that i) the fully automated preparation and quality control of clinical grade [^{18}F]AV-45; ii) [^{18}F]AV-45 had specific uptake by the amyloid plaque in post-operative MTC tissue; iii) [^{18}F]AV-45 PET/CT successfully detected the metastatic lymph lesion in a recurrent MTC patient. Whereas, [^{18}F]FDG PET/CT gave false positive diagnosis of several lymph lesions in the same patient.

Experimental Section

General information

Paraffin-embedded human medullary thyroid carcinoma (MTC) tissue samples from six patients and paraffin-embedded healthy human thyroid tissue samples were generously provided by the Department of Pathology, the First Affiliated Hospital of Dalian Medical University. The MTC samples

were cut into 3~5 μm thick sections and used immediately after de-paraffinization. The presence of amyloid plaque was determined by two senior pathologists independently. Fluoride-18 was produced by a Seimens Eclipse RD Cyclotron. [^{18}F]AV-45 was prepared with a Trasis allinone automated synthesizer. PET/CT imaging were acquired by a Seimens Biograph64 PET/CT scanner.

Ethics approval and consent to participate

Ethics approval (YJ-KY-FB-2020-26) for using patients' imaging data and post-surgical tissue was obtained from the Institute Research Medical Ethics Committee of First Affiliated Hospital of Dalian Medical University. The patient involved in this study had given a written consent.

Human participants

Four volunteers age between 42-65 without thyroid disease history participated in the [^{18}F]AV-45 PET/CT imaging study as control group. One recurrent MTC patient (62 year-old male) who had previously received thyroidectomy participated in the [^{18}F]FDG and [^{18}F]AV-45 PET/CT Imaging comparison study.

Automated preparation, purification, formulation and quality control of [^{18}F]AV-45

In a Trasis allinone automated synthesizer, fluoride-18 (~40 GBq) was trapped on a QMA cartridge (pre-activated with 10 mL 1.0 M $NaHCO_3$ and 10 mL sterilised water) and then eluted with a solution of Kryptofix®222 (25 mg)/K_2CO_3 (5 mg) in AcCN/H_2O (4/1 v/v, 0.5 mL) to the reaction vial. Water was removed by two rounds of azeotropic distillation with anhydrous AcCN (2 × 0.5 mL) at 110 °C. A solution of precursor, AV-105 (1 mg) in anhydrous DMSO (1.0 mL) was added to the reaction vial and heated at 110 °C for 10 min. The reaction was cooled to 60 °C before addition of 3 M HCl (0.8 mL) for deprotection. The reaction was heated at 120 °C for 5 min, cooled to RT, to which 1 M NaOH (2.5 mL) and sodium ascorbate (6.5 mL, 5 mg/mL) was added to neutralize to pH 7.0. The crude reaction mixture was purified by a built-in liquid chromatography using a C18-HPLC column (Waters XBridge Prep, 5 μm, 4.6 x 150 mm). The mobile phase is AcCN/H_2O (10 : 9) containing sodium ascorbate (5 mg/mL) and NH_4OAc (0.73 mg/mL) with a flow rate of 5 mL/min. The retention time of [^{18}F]AV-45 is 6.5 min. The [^{18}F]AV-45 was diluted with saline (20 mL), trapped on a tC18 cartridge and released with ethanol (1 mL) into a collection vial containing saline (10 mL) with sodium ascorbate (5 mg/mL). The solution was filtered by a 0.22 μm Millipore sterile filter into a sterile vial for injection. The chemical and radiochemical purity and molar activity of [^{18}F]AV-45 was determined using an Agilent 1200 HPLC with a Raytest GABI Star radioactivity detector, a diode array UV detector, and a ZORBAX Eclipse HPLC column (XDB-C18, 4.6 X 150 mm, 5 μm) with mobile phase of AcCN/H_2O (11 : 9) with a flow rate of 1.0 mL/min. Kryptofix was determined by the kryptofix spot test with silica based thin-layer chromatography (TLC). Discoloration

of the TLC was compared with a kryptofix reference solution (25 mg/mL). Radionuclide purity was determined with a germanium detector. Radionuclide identity is determined for the gamma spectrum emitted by the [^{18}F]AV-45. The half-life of radionuclide was measured by the radioactive decay of [^{18}F]AV-45 over time. Solvent residual was determined with gas chromatography. Sterility tests were performed by adding the decayed [^{18}F]AV-45 to tryptic soy broth (TBS) medium (Soya-bean casein digest) for two weeks at 25 °C. Bacterial endotoxin was determined using Endotoxin Assay Kits (Genescript).

Hematoxylin and eosin (H&E) staining

The dewaxed and hydrated human MTC tissue sections were incubated with alum haematoxylin solution at room temperature (RT) for 5 min before sequentially rinsing with distilled water for 1 min, 1% HCl in ethanol for 20 seconds, and distilled water for 1 min. The sections were then incubated with 0.5% eosin at RT for 2 min, rinsed with distilled water for 1 min, dehydrated, and mounted with glycerol before observation under a Nikon Eclipse E600 microscope with a Nikon DXM 1200 digital camera (Nikon, JP).

Congo red staining

The dewaxed and hydrated human MTC tissue sections were incubated with alum haematoxylin solution at RT for 2 min and then in 0.5% HCl in ethanol for 20 seconds before rinsing with distilled water twice for 5 min. The sections were then incubated in 1% Congo Red solution at RT for 25 min, rinsed with distilled water for 2 min, dehydrated, and mounted with glycerol before observation under a Nikon Eclipse E600 microscope with a Nikon DXM 1200 digital camera (Nikon, JP).

[^{18}F]AV-45 autoradiography and blocking study

The dewaxed and hydrated human MTC tissue sections were incubated in [^{18}F]AV-45 PBS solution (0.37 MBq/mL) with or without its non-radioactive reference compound (125 μg/mL) for 40 min at room temperature. The sections were then washed with distilled water and air dried prior to exposure to a multisensitive phosphor screen (PerkinElmer AQ5) at RT for 1 h. The phosphor screen was then scanned in a GE Amersham™ Typhoon™ Biomolecular Imager at a resolution of 25 μm. The images were analyzed with ImageQuant TL 8.1 software.

[^{18}F]AV-45 PET/CT Imaging of healthy human subjects

Four healthy volunteers (42-65 year old) free from thyroid diseases were intravenously injected [^{18}F]AV-45 (~300 MBq) and rested for 1 h before PET/CT scan. For anatomic correlation and attenuation correction of PET images, a low dose CT (120 kV, 35~170 mAs) was acquired from the vertex of the skull to the proximal femora. Subsequently, a PET scan of the same area was acquired with 2 min per bed position over 7 bed positions.

[^{18}F]FDG and [^{18}F]AV-45 PET/CT imaging of a MTC patient

A MTC patient (62 year old, male) was intravenously injected with [^{18}F]FDG in a dose of 5.55 MBq/Kg after 6 h of fasting and then rested for 1 h before PET/CT scan. The patient's blood sugar level was measured as 4.9 mM. Four days later, the same patient was received [^{18}F]AV-45 (278 MBq) and rested for 1 h before PET/CT scan. For anatomic correlation and attenuation correction of PET images, a low dose CT (120 kV, 35~170 mAs) was acquired from the vertex of the skull to the proximal femora. Subsequently, a PET scan of the same area was acquired with 2 min per bed position over 7 bed positions. The images were reconstructed using True X with a 168 x 168 matrix size, ordered-subsets expectation maximization (three iterations, 21 subsets, zoom 1) and post filter full-width at half-maximum of 4 mm. Quantitative image analysis was based on the transaxial frames of [^{18}F]FDG or [^{18}F]AV-45 series images by drawing the Region of Interest (ROI) and then measuring the maximum standardized uptake values (SUVmax) of radioactivity uptake in the neck. On the DICOM reconstructed images, a ROI in the neck was used to measure the lymph nodes and muscle SUVs.

Results

[^{18}F]AV-45 automated radiosynthesis, purification, formulation, and quality control

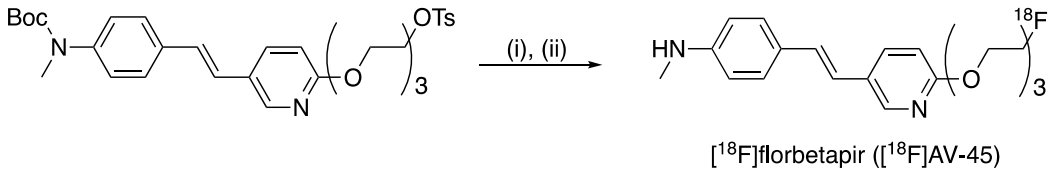

[^{18}F]florbetapir ([^{18}F]AV-45)

Scheme 1. Radiosynthesis of [^{18}F]AV-45 (i) ^{18}F, K_{222}, DMSO, 110 °C, 10 min; (ii) 3 M HCl, 120 °C, 5 min.

The fully automated radiosynthesis of [^{18}F]florbetapir ([^{18}F]AV-45) was achieved from the ^{18}F-labeling of AV-105 by a one-port two steps procedure on an Trasis Allinone synthesizer (**Scheme 1, Figure S1, and S2** for a photo of Trasis Allinone automated synthesizer and a photo of [^{18}F]-AV45 radiosynthesis module control diagram). The overall preparation time was within 60 min from the end of bombardment till formulation. The non-decay correct radiochemical yields of [^{18}F]AV-45 were 23.7±1.2%, (n = 3) with radiochemical purity >99% (supporting information **Figure S3** for QC HPLC chromatogram). The molar activity of [^{18}F]AV-45 were 401±84 GBq/μmoL, (n = 3) when starting with around 40 GBq of fluoride-18. The purified [^{18}F]AV-45 was formulated in injection saline containing 5 mg/mL of sodium ascorbate and 10% ethanol with pH around 6.5. The gamma energy and radionuclide purity of [^{18}F]AV-45 was 511 keV and 99%, respectively. The half-life was measured as 108 min. The Kryptofix222 was < 25 mg/L in the final formulation. The [^{18}F]AV-45 formulation was sterile and the endotoxin was < 0.006 EU/mL.

[^{18}F]AV-45 detected the amyloid plaques in MTC tissue sections

To confirm the presence of amyloids in MTC, continued tumor sections from five MTC patients excised by surgery were stained with the Congo Red and hematoxylin and eosin (H&E), respectively. Healthy

human thyroid tissue sections were also stained accordingly as negative control. Amyloid plaques were detected in all five tumor specimens as brown clusters by Congo Red and as pink clusters by H&E under the bright-field microscope indicated by the red arrows (**Figure 1 a, b** and **c, d**). Whereas, no amyloid deposition was observed in the healthy human thyroid tissue sections (**Figure 1 g, h** and **i, j**). Next, we investigated the selectivity and specificity of [^{18}F]AV-45 to bind to the MTC amyloid plaques in the continued tumor sections from the same five MTC patients by autoradiography. Continued healthy human thyroid tissue sections from the same specimens were also incubated with [^{18}F]AV-45 as negative control. The corresponding blocking experiments were conducted in the presence of the non-radioactive reference compound of [^{18}F]AV-45. Localized radioactivity accumulation was observed in the continued MTC tumor sections in the autoradiography images. The distribution of radioactivity is in good agreement with the amyloid plaques detected by the Congo Red and H&E staining. (**Figure 1 e**) The selective radioactivity accumulation in the amyloid plaques was largely blocked by the non-radioactive reference compound of [^{18}F]AV-45 (**Figure 1 f**). In contrast, there was little specific uptake of [^{18}F]AV-45 by the healthy human thyroid tissue sections (**Figure 1 k** and **l**). Subsequently, the [^{18}F]AV-45 uptake by the healthy human thyroid tissue sections and MTC tissue sections without or with blocking were quantified. The average [^{18}F]AV-45 uptake by the MTC tissue sections is 3.09 and 13.17 folds of those by the healthy human thyroid tissue sections and by the MTC tissue sections in the blocking experiments, respectively (**Figure 1 m**).

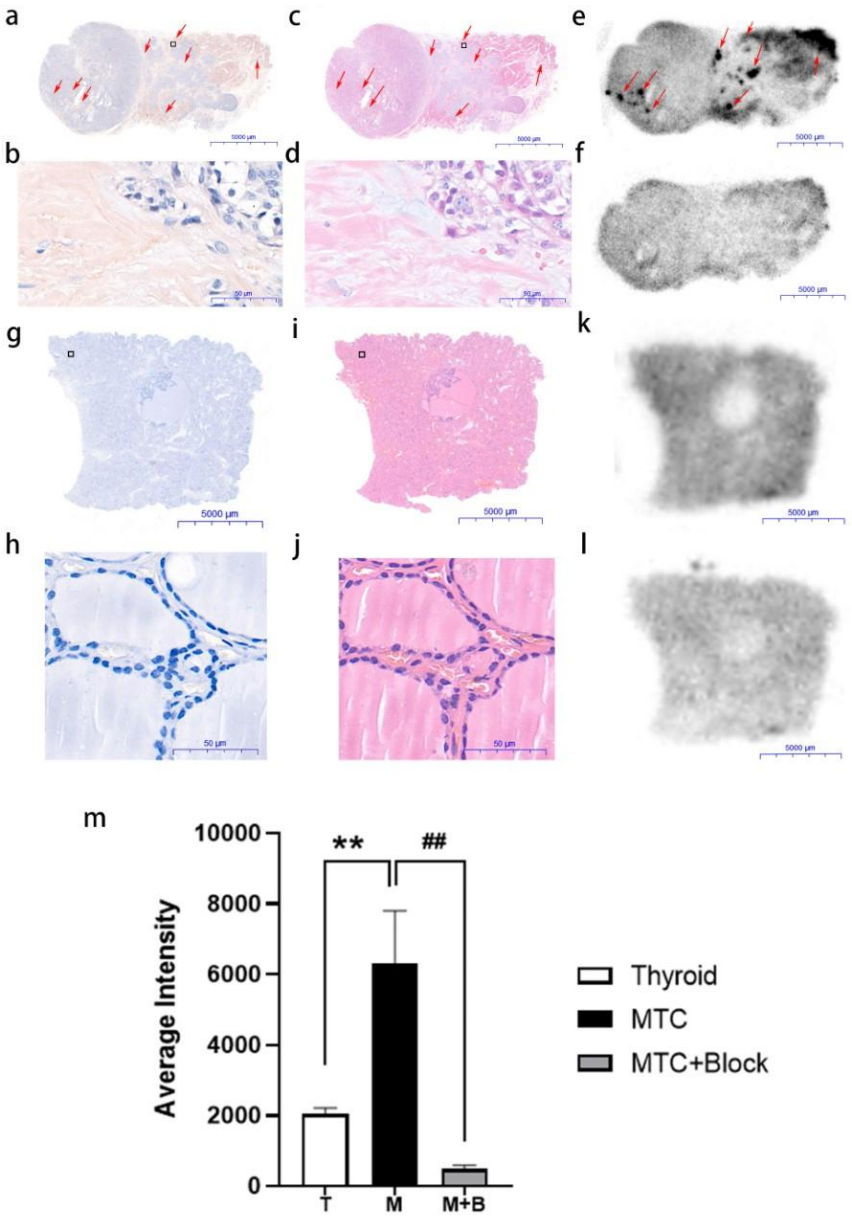

Figure 1. Representative images of continued tissue sections from a MTC tumor (a-f) and a healthy thyroid (g-l). (**a, g**) Congo Red staining; (**b, h**) 100X magnification of Congo Red staining; (**c, i**) H&E staining; (**d, j**) 100X magnification of H&E staining; (**e, k**) [^{18}F]AV-45 in vitro autoradiography; (**f, l**) [^{18}F]AV-45 in vitro autoradiography with co-incubation with the non-radioactive reference compound; (**m**) the average radioactivity intensity in tissue sections of healthy thyroids, and MTC and MTC with blocking from five patients, **p<0.01, $^{\#\#}$p<0.01. Images and data are representative of five independent experiments.

[^{18}F]AV-45 PET/CT imaging of healthy human subjects

Four human volunteers free from thyroid diseases were subjected to [^{18}F]-AV-45 PET/CT scan. The SUVmax values of thyroids, neck lymph nodes, and neck muscle were determined and summarized in

Table 1. The thyroid SUVmax values are close to 1.0. The neck lymph nodes SUVmax values are between 0.70-1.50. The neck muscle SUVmax values range from 0.90-1.33. No specific [^{18}F]-AV-45 retention was observed in these tissue. **(Figure 2)**

Table 1. Characteristics of healthy human subjects in the [^{18}F]-AV-45 PET imaging study

	age (years)	gender	thyroid SUVmax	neck lymph node 1 SUVmax	neck lymph node 2 SUVmax	neck muscle SUVmax
1	43	M	1.07	0.97	0.98	1.07
2	65	F	0.97	1.50	1.30	1.33
3	56	M	0.90	1.50	1.20	0.90
4	42	M	1.10	0.70	0.80	1.20

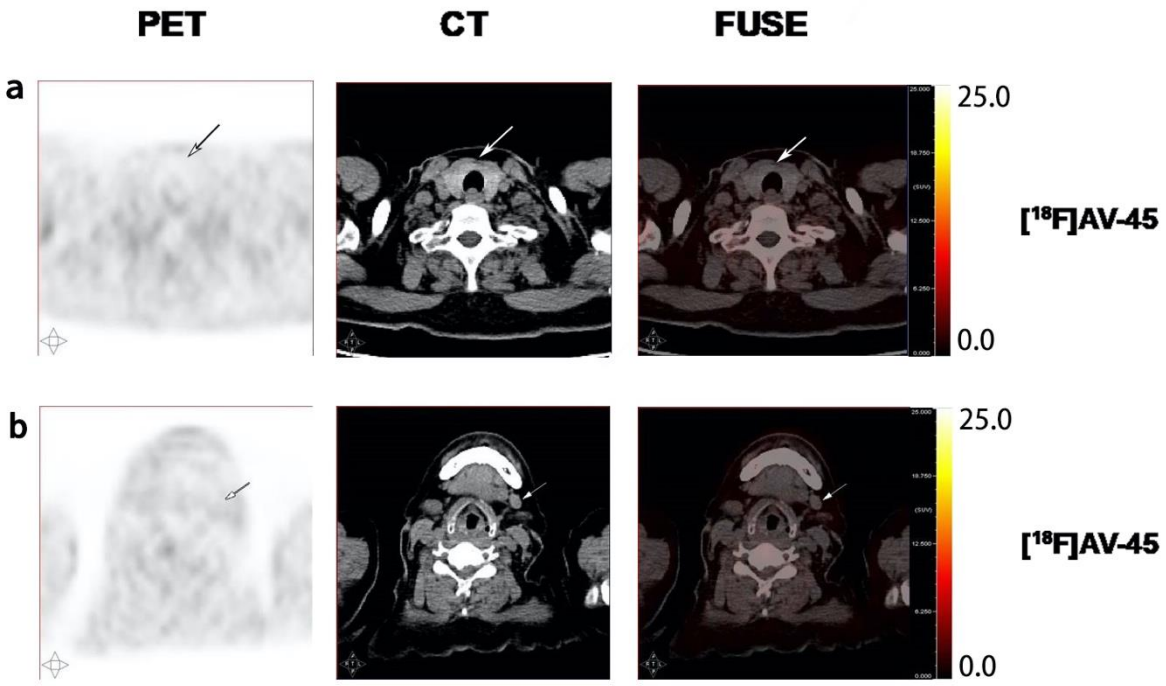

Figure 2. [^{18}F]AV-45 PET/CT images of a healthy human subject. Images are representative of four healthy volunteers. **(a)** thyroid; **(b)** lymph nodes.

Comparison of ^{18}F-FDG and [^{18}F]AV-45 PET/CT imaging of a MTC patient with recurrent neck lymph node metastasis

The calcitonin level (normal value <18.2 pg/mL) of a 62 year-old male patient with MTC history was increased to 4246 pg/mL. The [^{18}F]FDG PET/CT imaging detected elevated radioactivity uptake by multiple neck lymph nodes with SUVmax of 4.9, 3.4, and 2.8, respectively, indicated by the arrows (**Figure 3 a-c**). In contrast, only one of these lymph nodes showed increased [^{18}F]AV-45 uptake with

SUVmax of 2.5 and the other two [^{18}F]FDG positive lymph nodes had [^{18}F]AV-45 uptake closes to the background level with SUVmax of 0.9 and 1.0, respectively, in the PET/CT scan indicated by the arrows (**Figure 3 a-c**). However, the radioactivity distribution patterns in the ^{18}F-FDG and [^{18}F]AV-45 positive lymph node were different (**Figure 3 a**). The patient was subsequently received a radical neck dissection to remove all the left side neck lymph nodes that were then analysed by histopathology. The patient's calcitonin level was reduced to 326 pg/mL two months post-surgery and with no detectable disease at the time of this report.

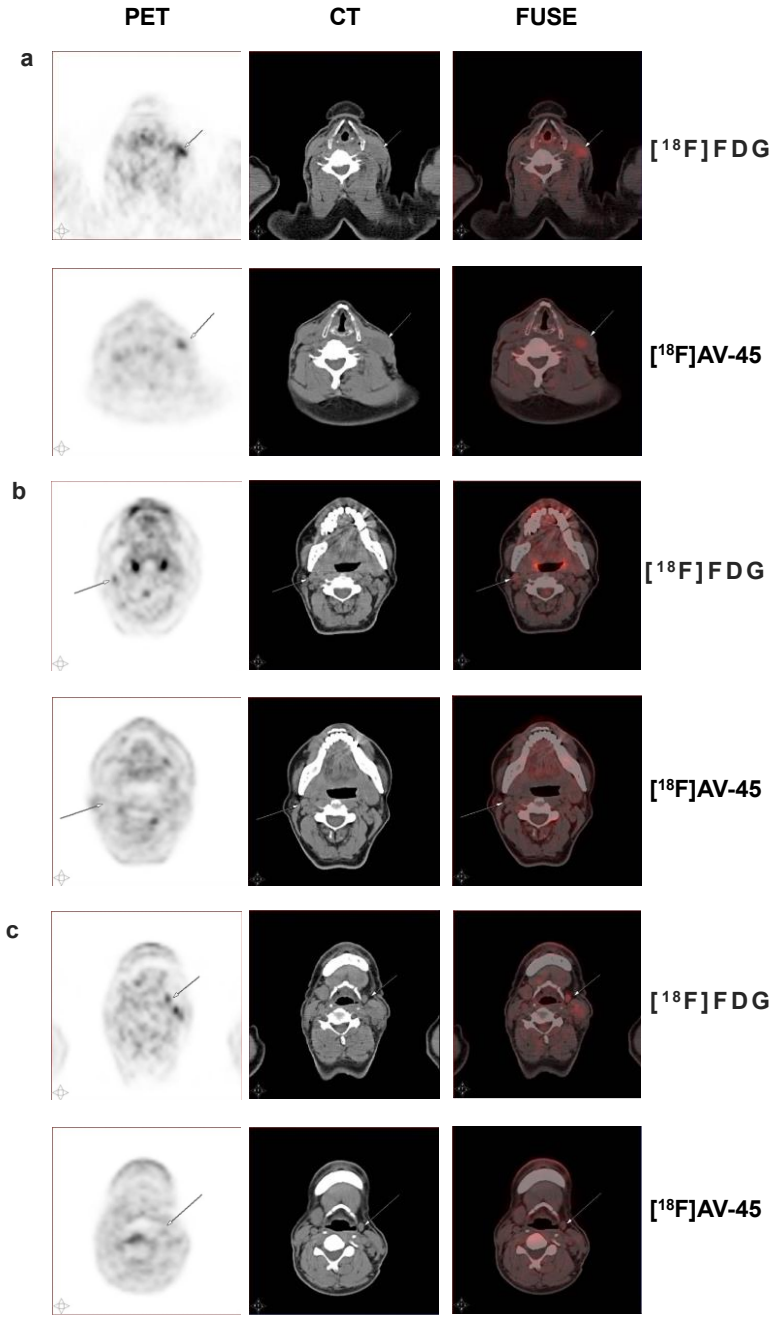

Figure 3. [^{18}F]FDG and [^{18}F]AV-45 PET/CT images of a MTC patient with recurrent neck lymph node metastasis. (a) MTC positive lymph node; (b, c) MTC negative lymph nodes.

Post-operative histopathological analysis confirmed [^{18}F]AV-45 PET positive lymph node as MTC with amyloid plaques

The excised tissues from the above MTC patient including all left side cervical lymph nodes and adhesion muscle were subjected to histopathological examination by Congo Red and H&E staining. The [^{18}F]AV-45 PET positive lymph node was confirmed as MTC, in which amyloid plaques were observed (**Figure 4 a-d**). The [^{18}F]AV-45 PET negative lymph nodes and adhesion muscle was MTC negative and free from amyloid plaques (**Figure 4 g-j and m-p**). *Ex vivo* [^{18}F]AV-45 autoradiography and the corresponding blocking study were also performed with the continued tissue sections of the above excised tissues. Localized radioactivity uptake was only observed in the [^{18}F]AV-45 PET positive lymph node tissue sections (**Figure 4 e**). The distribution of radioactivity uptake correlated to the amyloid plaques detected by both Congo Red and H&E staining. Additionally, the radioactivity uptake was largely blocked by the non-radioactive reference compound of [^{18}F]AV-45 (**Figure 4 f**). While, the [^{18}F]AV-45 uptake by the lymph nodes and paratumor muscle sections free from MTC was minimal (**Figure 4 k and q**).

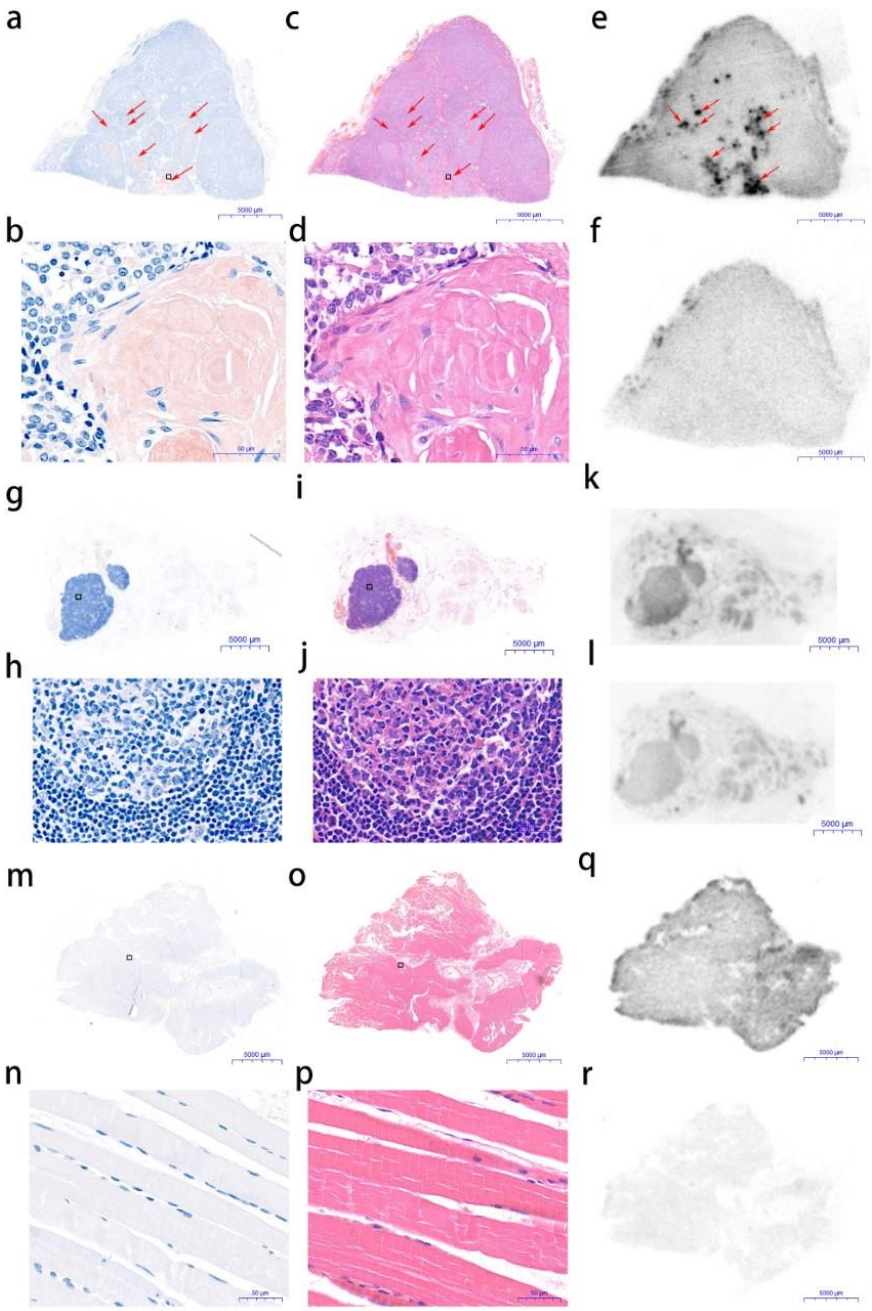

Figure 4 Post-operative histopathological analysis of the metastatic lymph node (a-f), non-metastatic lymph nodes (g-l), and paratumor muscle tissue sections (m-r) from the MTC patient of [^{18}F]AV-45 PET imaging. (**a, g, m**) Congo Red staining; (**b, h, n**) 100X magnification of Congo Red staining; (**c, i, o**) H&E staining; (**d, j, p**) 100X magnification of H&E staining; (**e, k, q**) [^{18}F]AV-45 autoradiography; (**f, l, r**) [^{18}F]AV-45 autoradiography with co-incubation of the non-radioactive reference compound. Images are representative of three independent experiments.

Discussion

Despite of its rarity, MTC is the most fatal thyroid cancer with a high recurring rate.[2] The early diagnosis of MTC can significantly improve patients' prognosis.[3] Recently, [^{18}F]FDOPA has shown superior

sensitivity and selectivity towards recurrent MTC.[10] However, the challenging radiochemical preparation of [^{18}F]FDOPA severely limited its clinical availability.[11] Thus, an alternative PET tracer that can be ready prepared on a standard automated synthesizer is required. Amyloid deposition has been recognized as one of the characteristic pathology of MTC. The main composition of MTC amyloid is formed from the misfolding of calcitonin that contains β-sheets in its secondary structure,[15] which makes it an attractive target for molecular imaging. In recent studies, β-amyloid targeting radiotracers such as [^{18}F]AV-45 and [^{18}F]FDDNP for AD PET imaging have been demonstrated as promising contrast reagents for the detection of cardiac amyloidosis[16] and pancreatic islet amyloid,[17] respectively. [^{18}F]AV-45 is a specific molecular probe for β-amyloid, while, [^{18}F]FDDNP binds to both β-amyloid and tangled tau proteins.[18] In addition, in our lab, we have implemented the fully automated preparation of clinical grade [^{18}F]AV-45 with good and reproducible RCYs. Thus, we decided to apply [^{18}F]AV-45 to the diagnosis of recurrent MTC with clinical PET/CT imaging.

Initially, to produce clinical grade [^{18}F]AV-45, we developed the automated radiochemical preparation, purification, and formulation of [^{18}F]AV-45 on a Trasis Allinone radiosynthesizer. [^{18}F]AV-45 is routinely produced in multiple patient dose with this fully automated procedure. The quality control indicates that [^{18}F]AV-45 produced meets the European Pharmacopoeia standard for radiopharmaceuticals. Next, we tested [^{18}F]AV-45 on tissue sections from five different MTC patients and healthy human thyroid tissue samples as negative control. Amyloid deposition was confirmed by both Congo Red and H&E staining. Localized accumulation of [^{18}F]AV-45 in the tissue sections of all five MTC patients was observed. The distribution of the radioactivity in these tissue sections had similar patterns of Congo Red and H&E staining. Moreover, the radioactivity can be largely blocked by the [^{18}F]AV-45 non-radioactive reference compound. In contrast, the [^{18}F]AV45 had little uptake by the healthy human thyroid tissue. These results demonstrate that [^{18}F]AV-45 can selectively and specifically accumulate in the MTC amyloid plaques. To ensure [^{18}F]AV-45 has no specific accumulation in the healthy neck tissues including thyroid, lymph nodes, and muscle, we conducted [^{18}F]AV-45 PET/CT imaging study with four volunteers without thyroid disease history. Only background level of radioactivity was observed in the thyroids, neck lymph nodes, and muscle from all four volunteers. Encouraged by these results, we compared the use of [^{18}F]FDG and [^{18}F]AV-45 PET/CT imaging for the detection of metastasis in a recurrent MTC patient. Several neck lymph nodes with increased [^{18}F]FDG uptake were observed. While, only one of them showed increased [^{18}F]AV-45 uptake in the PET imaging studies. All these lymph nodes were removed by surgery. Post-operative histopathological analysis with Congo Red and H&E staining confirmed that the [^{18}F]AV-45 positive lymph node had MTC metastasis with amyloid plaque deposition. In contrast, the [^{18}F]AV-45 negative lymph nodes were free from MTC with no amyloid plaques detected. It is well documented in the literature that [^{18}F]FDG can give false positive diagnosis of lymph node metastasis due to local inflammation.[19,20] In this recurrent MTC patient, [^{18}F]FDG cannot differentiate the metastatic lymph nodes from the inflammation lymph nodes. While, [^{18}F]AV-45 clearly has the specificity to detect MTC lymph node metastasis. The patient's calcitonin level was rapidly decreased post the radical neck dissection and free from MTC at the time of this report. It is worth noting that the

[^{18}F]AV-45 uptake is related to the degree of amyloid deposition in the MTC. While, the [^{18}F]FDG uptake is correlated to the expression and function of the glucose transport proteins and the intracellular hexokinase. Due to the different accumulation mechanisms, the radioactivity distributions of [^{18}F]AV-45 and the [^{18}F]FDG on the same MTC positive lymph node were not completely overlapped. The key limitation of this pilot clinical study is that only one MTC patient was recruited and imaged with [^{18}F]AV-45. Currently, we are preparing to expand the pilot clinical study to exam the sensitivity of [^{18}F]AV-45 for MTC diagnosis with larger patient population. We expect that [^{18}F]AV-45 would be a valuable PET tracer for not only the diagnosis of MTC but monitoring the therapeutic efficacy of MTC chemo- and radio-therapies. For example, several ^{111}In and ^{177}Lu labelled cholecystokinin-2 receptor targeting minigastrin (MG) peptide analogues have shown great promise for MTC theranostic applications.[21,22] As [^{18}F]AV-45 has different molecular mechanism for MTC uptake to these MG peptides, it would be sensible to conduct a comparison study to investigate the sensitivity and reliability between [^{18}F]AV-45 and radiolabelled MG peptides to monitor the peptide receptor radionuclide therapies.

Conclusion

In this first in human pilot clinical study, we have demonstrated that [^{18}F]AV-45 has selective and specific uptake by the amyloid plaques in MTC tissue samples. [^{18}F]AV-45 PET/CT imaging successfully detected MTC lymph node metastasis in a recurrent MTC patient. In contrast, [^{18}F]FDG gave false positive results for multiple lymph node metastasis. These results warrant further assessment of [^{18}F]AV-45 for MTC diagnosis with PET/CT imaging.

References

1. Pacini, F.; Castagna, M.G.; Cipri, C.; Schlumberger, M. Medullary thyroid carcinoma. *Clin. Oncol.* **2010**,22(6), 475–485.

2. Skoura, E. Depicting medullary thyroid cancer recurrence: the past and the future of nuclear medicine imaging. *Int. J. Endocrinol. Metab*. **2013**, 11, e8156.

3. Modigliani, E.; Cohen, R.; Campos, J.M.; Conte-Devolx,B.; Maes, B.; Boneu, A.; Schlumberger, M.; Bigorgne, J.C.; Dumontier, P.; Leclerc, L.; Corcuff, B.; Guilhem, I. Prognostic factors for survival and for biochemical cure in medullary thyroid carcinoma: results in 899 patients. The GETC study group. Groupe d'etude des tumeurs a calcitonine. *Clin. Endocrinol*. **1998**, 48, 265–273.

4. Trimboli, P.; Treglia, G.; Guidobaldi, L.; Romanelli, F.; Nigri, G.; Valabrega, S.; Sadeghi, R.; Crescenzi, A.; Faquin, W.C.; Bongiovanni, M.; Giovanella, L. Detection rate of FNA cytology in medullary thyroid carcinoma: a meta-analysis. *Clin. Endocrinol*. **2015**, 82, 280–285.

5. Koopmans, K.P.; Neels, O.N.; Kema, I.P.; Elsinga, P.H.; Links, T.P.; de Vries, E.G.; Jager, P.L. Molecular imaging in neuroendocrine tumors: molecular uptake mechanisms and clinical results. *Crit. Rev. Oncol.*

Hematol. **2009**, 71, 199–213.

6. Clarke, S.E.; Lazarus, C.R.; Wraight, P.; Sampson, C.; Maisey, M.N. Pentavalent [^{99m}Tc]DMSA, [^{131}I]MIBG, and [^{99m}Tc]MDP–an evaluation of three imaging techniques in patients with medullary carcinoma of the thyroid. *J. Nucl. Med*. **1988**, 29, 33–38.

7. Kwekkeboom, D.J.; Reubi, J.C.; Lamberts, S.W.; Bruining, H.A.; Mulder, A.H.; Oei, H.Y.; Krenning, E.P. In vivo somatostatin receptor imaging in medullary thyroid carcinoma. *J. Clin. Endocrinol. Metab*. **1993**,76,1413–1417.

8. Treglia, G.; Castaldi, P.; Villani, M.F.; Perotti, G.; de Waure, C.; Filice, A.; Ambrosini, V.; Cremonini, N.; Santimaria, M.; Versari, A.; Fanti, S.; Giordano, A.; Rufini, V. Comparison of ^{18}F-DOPA, ^{18}F-FDG and ^{68}Ga-somatostatin analogue PET/CT in patients with recurrent medullary thyroid carcinoma. *Eur. J. Nucl. Med. Mol. Imaging*. **2012**, 39, 569–580.

9. Lee, S.W.; Shim, S.R.; Jeong, S.Y.; Kim, S.J. Comparison of 5 different PET radiopharmaceuticals for the detection of recurrent medullary thyroid carcinoma: a network Meta-analysis. *Clin. Nucl. Med*. **2020**, 45, 341–348.

10. Giovanella, L.; Treglia, G.; Iakovou, I.; Mihailovic, J.; Verburg, F.A.; Luster, M. EANM practice guideline for PET/CT imaging in medullary thyroid carcinoma. *Eur. J. Nucl. Med. Mol. Imaging*. **2020**, 47, 61–77.

11. Mossine, A.V.; Tanzey, S.S.; Brooks, A.F.; Makaravage, K.J.; Ichiishi, N.; Miller, J.M.; Henderson, B.D.; Erhard, T.; Bruetting, C.; Skaddan, M.B.; Sanford, M.S.; Scott, P. Synthesis of High-Molar-Activity [^{18}F]-6-Fluoro-L-DOPA Suitable for Human Use via Cu-Mediated Fluorination of a BPin Precursor. *Nat. Protoc.* **2020**, 15, 1742–1759.

12. Sipe, J. D.; Cohen, A.S. Review: history of the amyloid fibril. *J. Struct. Biol.* **2000**, 130, 88–98.

13. Nelson, R.; Sawaya, M.R.; Balbirnie, M.; Madsen, A.Ø.; Riekel, C.; Grothe, R.; Eisenberg, D. Structure of the cross-β spine of amyloid-like fibrils. *Nature*. **2005**, 435,773–778.

14. Liu, Y.; Zhu, L.; Plössl, K.; Choi, S. R.; Qiao, H.; Sun, X.; Li, S.; Zha, Z., Kung, H.F. Optimization of automated radiosynthesis of [^{18}F]AV-45: a new PET imaging agent for Alzheimer's disease. *Nucl. Med. Biol.* **2010**, 37, 917–925.

15. Khurana, R.; Agarwal, A.; Bajpai, V.K.; Verma, N.; Sharma, A.K.; Gupta, R.P.; Madhusudan, K.P. Unraveling the amyloid associated with human medullary thyroid carcinoma. *Endocrinology* **2004**, 145(12), 5465–5470.

16. Dorbala S.; Vangala D.; Semer J.; Bruyere Jr. J. R.; Carli M. F Di.; Moore S. C.; Falk R. H. Imaging cardiac amyloidosis: a pilot study using ^{18}F-florbetapir positron emission tomography. *Eur. J. Nucl. Med. Mol. Imaging* **2014**, 41, 1652-1662;

17. Lu, Z.; Xie, J.; Yan, R.; Yu, Z.; Sun, Z.; Yu, F.; Gong, X.; Feng, H.; Lu, J.; Zhang, Y. A pilot study of pancreatic islet amyloid PET imaging with [^{18}F]FDDNP. *Nucl. Med. Commun.* **2018**, *39* (7), 659– 664;

18. Shoghi-Jadid, K.; Small, G. W.; Agdeppa, E. D.; Kepe, V.; Ercoli, L. M.; Siddarth, P.; Read, S.; Satyamurthy, N.; Petric, A.; Huang, S. C.; Barrio, J. R. Localization of neurofibrillary tangles and beta-amyloid plaques in the brains of living patients with Alzheimer disease. *Am. J. Geriatr. Psych.***2002**, *10,* 24–35

19. Endoh, H.; Yamamoto, R.; Ichikawa, A.; Shiozawa, S.; Nishizawa, N.; Satoh, Y.; Oriuchi, N. Clinicopathologic Significance of False-Positive Lymph Node Status on FDG-PET in Lung Cancer. *Clin. Lung. Cancer*. **2020**, S1525-7304(20)30142-X.

20. Di Martino, E.; Nowak, B.; Krombach, G.A.; Sellhaus, B.; Hausmann, R.; Cremerius, U.; Büll, U.; Westhofen, M. Results of pretherapeutic lymph node diagnosis in head and neck tumors. Clinical value of ^{18}-FDG positron emission tomography (PET). *Laryngorhinootologie* **2000**, 79(4), 201-206.

21. Rangger, C.; Klingler, M.; Balogh, L.; Pöstényi, Z.; Polyak, A.; Pawlak, D.; Mikołajczak, R.; von Guggenberg, E. ^{177}Lu Labeled Cyclic Minigastrin Analogues with Therapeutic Activity in CCK2R Expressing Tumors: Preclinical Evaluation of a Kit Formulation. *Mol. Pharm.* **2017**, *14*, 3045–3058.

22. Klingler, M.; Decristoforo, C.; Rangger, C.; Summer, D.; Foster, J.; Sosabowski, J.K.; von Guggenberg, E. Site-specific stabilization of minigastrin analogs against enzymatic degradation for enhanced cholecystokinin-2 receptor targeting. *Theranostics* **2018**, *8*, 2896–2908.

ASSOCIATED CONTENT

Supporting information:

AV-105 Characterization: ^{1}HNMR, High resolution MS, and HPLC chromatogram

Figure S1. Trasis Allinone automated synthesizer with [^{18}F]AV45 cassette

Figure S2. Trasis Allinone automated synthesizer [^{18}F]AV45 radiosynthesis module control diagram.

Figure S3. Quality control of [^{18}F]-AV-45. HPLC chromatogram of non-radioactive reference compound (above); HPLC chromatogram of purified [^{18}F]-AV-45 (below).

AUTHOR INFORMATION

Corresponding authors:

Zhi Lu
Email: luzhi712@163.com
Address: Department of Nuclear Medicine, First Affiliated Hospital of Dalian Medical University, People's Republic of China, 116021;
Ran Yan
Email: ran.yan@kcl.ac.uk
Address: King's College London, School of Biomedical Engineering and Imaging Sciences, St. Thomas' Hospital, SE1 7EH, London, United Kingdom.

AUTHOR CONTRIBUTIONS

Chun Li and Pengxin Zhang contributed equally to this work. **Chun Li:** autoradiography, data collection and analysis, and manuscript preparation; **Pengxin Zhang:** Congo Red and H&E staining and histopathological analysis; **Ruirui Nie:** autoradiography, Congo Red and H&E staining**; Jinghui Xie:** PET imaging acquisition and data analysis; **Xiaoyan Gong:** [^{18}F]AV-45 and [^{18}F]FDG production and measurement of RCYs, radiochemical purity, and molar activity; **Zilin Yu:** autoradiography experiment design and supervision; **Ran Yan and Zhi Lu:** conceptualization, funding acquisition, supervision, and manuscript drafting. All authors read and approved the final manuscript.

NOTES

The authors report no conflicts of interest in this work.

FUNDING SOURCES

Natural Science Foundation of Liaoning Province of China (Grant no. 20180530048); the Royal Society for the International Exchanges Grant (IEC\NSFC\170006); the Wellcome/EPSRC Centre for Medical Engineering at King's College London [WT 203148/Z/16/Z]; the EPSRC Programme Grant, [EP/S032789/1].

ACKNOWLEDGMENTS

Zhi Lu thanks the support from Natural Science Foundation of Liaoning Province of China (Grant no. 20180530048). Ran Yan thanks the Royal Society for the International Exchanges Grant (IEC\NSFC\170006). The research was funded/supported by the National Institute for Health Research (NIHR) Biomedical Research Centre based at Guy's and St Thomas' NHS Foundation Trust and King's College London, the Wellcome/EPSRC Centre for Medical Engineering at King's College London [WT 203148/Z/16/Z], the King's College London and UCL Comprehensive Cancer Imaging Centre funded by CRUK and EPSRC in association with the MRC and DoH (England), the Experimental Cancer Medicine Centre at King's College and the King's Health Partners/ King's College London Cancer Research UK

Cancer Centre. This work was also supported by EPSRC Programme Grant, [EP/S032789/1].

ABBREVIATIONS

3,4-Dihydroxy-6-[^{18}F]fluoro-L-phenylalanine ([^{18}F)FDOPA)

2-Deoxy-2-[^{18}F]fluoro-D-glucose ([^{18}F]FDG)

Magnetic resonance imaging (MRI)

Medullary thyroid carcinoma (MTC)

Megabecquerel (MBq)

Positron emission tomography (PET)

Single-photon emission computed tomography (SPECT)

Standardized uptake value (SUV)

TABLE OF CONTENTS GRAPHIC